ANNALES
UNIVERSITATIS MARIAE CURIE-SKŁODOWSKA
LUBLIN – POLONIA

VOL. LVII, 7 SECTIO AA 2002

Packing transitions of Lennard Jones fluids in carbon slit pores

T.X. Nguyen, S.K. Bhatia[a)] and D. Nicholson[b)]
Department of Chemical Engineering
The University of Queensland
Brisbane, Qld. 4072, Australia

In this article we apply a recently developed density functional theory approach to the prediction of the temperature dependent variation in capacity with pore size of methane and carbon tetraflouride, and the associated packing transitions. The latter is an important compound as a member of the halocarbon family that are established greenhouse gas contributors. The capacities predicted by the proposed model are in good agreement with those obtained from grand canonical Monte Carlo simulation. Pair distributions reveal characteristic features that correspond to the sequence of buckling and rhombic transitions that occur as the slit pore width is increased.

1. INTRODUCTION

While in homogeneous bulk phase, molecules are isotropically packed and packing configuration is independent of the geometry and volume of the container, an adsorbed phase in confined geometry is not only inhomogeneous but also its packing configuration is dependent upon pore geometry, volume and solid-fluid interaction. This results in unique physical phenomena of an adsorbed phase in pores such as packing transitions and pore size dependent capacity, a reduction in critical temperature, as well hysteresis, which are not observed in bulk phases.

[a)] To whom correspondence may be addressed. Email: sureshb@cheque.uq.edu.au
[b)] Permanent address: Computational and Structural Group, Department of Chemistry, Imperial College, London SW72AY

Existing isotherm models are based on different approaches that have a kinetic, thermodynamic or statistical mechanical staring point. Most of the existing isotherm models contain one or more parameters that are related directly or indirectly to the capacity of the adsorbate in a pore. The capacity is defined as the density at the close packed limit which, in existing models, is considered to be a function only of temperature through the thermal expansion of the adsorbed fluid. This seems reasonable for an adsorbed fluid in large pores such as macropores or mesopores where capacity is independent of the pore volume. However this is not the case for micropores whose pore widths are only a few adsorbate molecular diameters. Here the close packed configuration of the adsorbed phase can vary with pore width, passing sequentially through hexagonal and square geometries, in a similar manner to that observed experimentally when colloid suspensions are confined between parallel glass plates [1-4]

In earlier work, Schmidt and Löwen [5] confirmed the dependence of closed packing density on plate separation distance, by means of theoretical studies and computer simulations of frozen hard sphere fluids between two parallel plates. Several studies also show pore size dependent density at high pressure due to packing transitions in all geometries [6-8]. The transitions occurring continuously with increasing pore width allow rearrangement of adsorbed molecules in pores in order to attain a minimum free energy configuration [6]. Although much theoretical work has been done on high pressure layering transitions in confined geometry, the studies have invariably involved only hard sphere systems such as colloidal particle systems where the capacity can be calculated purely from the geometry of the particles [5, 9]. Little theoretical study of high pressure layering transitions of soft sphere systems has been attempted due to their complexity.

In the present work our recent model [10] is applied to methane and carbon tetraflouride. For convenient reference, the paper is organized as follows: In the next section, we outline the theory and show how it is applied at close-packed limits in two or three dimensions. We derive specific expressions that predict the packing transitions and the associated structures that occur as pore width is increased. Section 3 gives a brief summary of the GCMC technique used in the computer simulations. In Section 4 we compare the results from the new theory with simulation data and demonstrate that it is capable of accurately predicting the structure and packing densities in filled pores. A summary and conclusions are given in Section 5.

2. MATHEMATICAL MODEL OF AN ADSORBED L-J FLUID IN A CARBON SLIT- PORE AT THE CLOSE PACKED LIMIT

General approach. We use density functional theory approach, which is a powerful tool to study adsorption equilibrium in a constrained space such as in pores[11-17]. This approach minimizes the grand potential [18]

$$\Omega[\rho] = F[\rho] + \int \rho(\mathbf{r})\left[v_{ex}(\mathbf{r}) - \mu\right]d\mathbf{r} \tag{1}$$

Here $\rho(\mathbf{r})$ is the density profile in the presence of external potential v_{ex}. Further, μ is the chemical potential of the adsorbate, and $F[\rho]$ is the intrinsic Helmholtz free energy, decomposed in terms of an ideal gas part $F_{id}[\rho]$ and an excess part $F_{ex}[\rho]$

$$F[\rho] = F_{id}[\rho] + F_{ex}[\rho] \tag{2}$$

Given suitable models for these free energies, the general procedure is to obtain the optimal profile $\rho(\mathbf{r})$ that minimizes the grand potential $\Omega[\rho]$ for the chosen system, such as the confined pore space.

Application to close-packed limits in 2D and 3D. In the close-packed limit the adsorbed phase is considered as a set of identical unit cells, which are detailed in a later section. The local density can be then be treated as the density in the unit cell. Consequently, eq.(1) can be rewritten in terms of unit cell potential as follows :

$$\Omega = F_{id} + F_{ex} + N(v_{ex} - \mu) = F_{id} + F_{ex} + Nv_{ex} - N\mu\,, \tag{3}$$

where N is the number of adsorbed molecules in a unit cell.
For the two dimensional unit cell, the ideal gas free energy is given by

$$F_{id} = NkT\left[\ln\left(N^*\lambda^2\right) - 1\right], \tag{4}$$

Here λ is the de Broglie wavelength, $\lambda = \sqrt{h^2/2\pi mkT}$, where h is Planck's constant, m is the mass of the adsorbate particle, k is Boltzmann's constant and T is temperature.

The (2D) density of the unit cell, N^*, is given by

$$N^* = \frac{N}{S} \ , \tag{5}$$

where N is the number of molecules in a unit cell, and S the surface area occupied on an adsorbent plane. The chemical potential may be expressed in terms of the bulk activity a, as

$$\mu = kT\ln(\lambda^3) + kT\ln(a)\,, \tag{6}$$

In eq. (3) the excess part of the Helmholtz free energy may be obtained from the canonical partition function, Q, through

$$F_{ex} = -kT\ln Q \ , \tag{7}$$

where

$$Q = g(N,M)e^{-\beta E} \tag{8}$$

Here, $g(N, M)$ is the degeneracy and M is the total number of adsorptive sites, while E is the total interaction potential energy of the unit cell, and $\beta = 1/kT$. In the close packed limit, only one configuration is expected, so that $g(N,M)=1$. The excess Helmholtz free energy is therefore given by

$$F_{ex} = E\,, \tag{9}$$

To proceed further it is necessary to specify the potential models and unit cell geometry that will be employed for minimization of the grand free energy Ω.

Potential models. *Adsorbate-adsorbate interaction potential.* The adsorbate-adsorbate interactions are described by a (L-J) 12-6 pair potential

$$\Phi_{ii}(r) = 4\varepsilon_{ii}\left[\left(\frac{\sigma_{ii}}{r}\right)^{12} - \left(\frac{\sigma_{ii}}{r}\right)^{6}\right] \ , \tag{10}$$

here ε_{ii} is well depth, σ_{ii} is molecular diameter for adsorbate. In what follows we have used the parameters, $\varepsilon_{ii}/k = 148.2\,\mathrm{K}$ and 134 K ; $\sigma_{ii} = 3.81$ Å and 4.662 Å as representatives of CH_4 and CF_4.

Solid-fluid interaction potential. The above model has been applied to adsorption in a carbonaceous slit-pore with the solid-fluid interaction, given by the 10-4-3 Steele potential[19]

$$\Phi_{si}(z) = A\left[\frac{2}{5}\left(\frac{\sigma_{si}}{z}\right)^{10} - \left(\frac{\sigma_{si}}{z}\right)^{4} - \left(\frac{\sigma_{si}^{4}}{3\Delta(0.61\Delta + z)^{3}}\right)\right], \tag{11}$$

where $A = 2\pi\rho_s\varepsilon_{si}\sigma_{si}^2\Delta$. z is the distance between an adsorbate molecule of species *i* and the solid surface. Δ is interplanar distance in the carbon and ρ_s is activated carbon density. The parameters, well depth ε_{si} and σ_{si}, are determined using the Lorentz-Berthelot mixing rules. The carbon parameters used in the study have the values[19] $\sigma_{ss} = 0.34nm$, $\varepsilon_{ss}/k = 28.0K$, $\Delta = 0.335nm$ and $\rho_s = 114nm^{-3}$. The external potential in a pore of width H (centre-to-centre distance of carbon atoms on opposing planes) is given by

$$v_{ex} = \Phi_{si}(z) + \Phi_{si}(H - z). \tag{12}$$

Unit cell energy. Using the above fluid- fluid and fluid-solid potential models, the total interaction energy E of a unit cell can now be constructed for any chosen transition. We consider close packed L-J particles forming a two-dimensional structure, comprising unit cells. To determine the total interaction potential for the unit cell, the following assumptions are applied

- Pairwise additivity.
- The adsorbed phase consists of an integral number of identical unit cells.
- Structural transitions of the adsorbed phase correspond to a series of following crystalline structures as the pore width increases, following

$1\Delta \rightarrow 2\square \rightarrow 2\Delta \rightarrow 3\square \rightarrow 3\Delta\ldots.$

The symbol Δ represents hexagonal packing and the symbol □ square packing, and the numbers preceding the symbols represent the number of layers in the adsorbed phase. This sequence of crystalline structure has been studied for hard sphere systems [6, 20] and two main transition types may be identified:

1. The transitions $n\square \rightarrow n\Delta$, or rhombic transitions. In this case, only the structure within each layer changes.
2. The transitions $n\square \rightarrow (n+1)\Delta$, or buckling transitions. In this case, a new layer is formed together with structural variation of the adsorbed phase.

Based on the above assumptions, the unit cells corresponding to each transition are presented in turn below:

Evolution of the monolayer and formation of a second layer. *Buckling transition* ($1\Delta \rightarrow 2\square$). Figure 1 depicts the transition occurring with increase in pore size when the number of adsorbed layers increases from one to two. At the smaller pore size when only one layer is formed, the particles are organized in hexagonal close-packed geometry. As the pore size increases, a continuous transition occurs to the square geometry attained when exactly two layers can be formed.

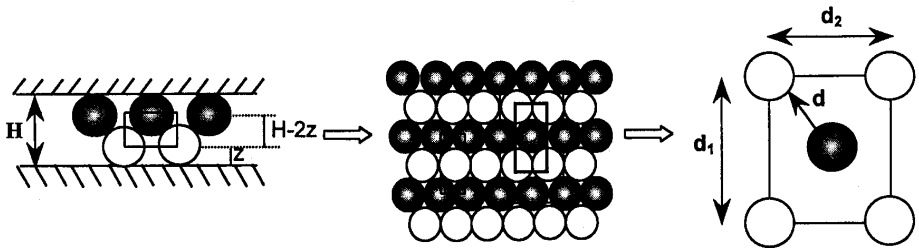

(a) (b) (c)

Fig. 1. Evolution of monolayer to form second layer. (a) The rows containing empty circles move down and those having filled balls move up when width increases. The rectangle represents the selected unit cell projected in different directions. (b) The hexagonal configuration is divided into two distinct types of rows.

From the Figure 1, each adsorbate molecule has the same number of nearest neighbors. Thus, the interaction potential E of the unit cell is given as follows:

$$E = N\left[\Phi_{ii}(d) + \Phi_{ii}(d_1) + \Phi_{ii}(d_2) + 2\Phi_{ii}(\sqrt{d_1^2 + d_2^2})\right], \tag{13}$$

where d, d_1, d_2 are the unit cell parameters identified in Figure 1(C), and N is the number of particles in the unit cell. Here N=2.

The relationship between the unit cell dimensions, d, d_1, d_2 and the pore width H, and density can be derived from the geometry of the unit cell (Figure 1).

$$d_1 = b_1\sqrt{2\left[d^2 - (H - 2z)^2\right]}, \tag{14}$$

$$d_2 = b_2\sqrt{2\left[d^2 - (H-2z)^2\right]}, \tag{15}$$

and the density per unit volume is given by

$$\rho_{1-2} = b_3 \frac{1}{H\left[d^2 - (H-2z)^2\right]}, \tag{16}$$

where

$$\alpha = \frac{d_2}{d_1}\ ;\ b_1 = \sqrt{\frac{2}{\alpha^2+1}}\ ;\ b_2 = \alpha\sqrt{\frac{2}{\alpha^2+1}} \text{ and } b_3 = \frac{\alpha^2+1}{2\alpha}. \tag{17}$$

Rhombic transition (*2□ → 2*Δ). Figure 2 describes the subsequent transition of the buckling transition, which ends up with exactly two layers, as pore width widens. In this transition, a continuous deformation of the square configuration into a hexagonal configuration occurs without the formation of a new layer.

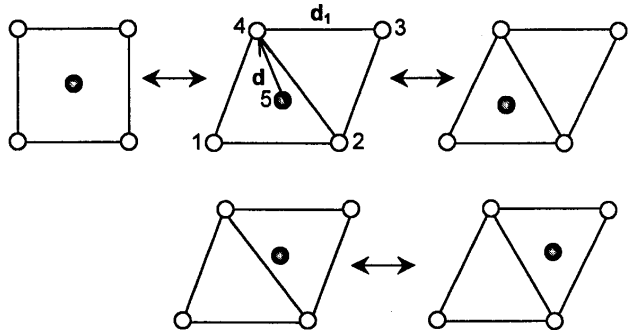

Fig. 2. Continuous deformation of a unit cell. Square configuration is continuously deformed to transform into hexagonal configuration as pore width enlarges. Empty circles represent adsorbate molecules in the first layer and filled ones adsorbate molecules in the second layer.

For the unit cell shown in the Figure 2, the total interaction *E* of the cell for the rhombic transition is given as follows:

$$E = N\left[2\Phi_{ii}(d_1) + \Phi_{ii}(d_{42}) + \Phi_{ii}(d_{31}) + 1.5\Phi_{ii}(d) + 0.5\Phi_{ii}(d_{53})\right], \tag{18}$$

where *N* is the number of molecules in the unit cell. In this case, *N* =2. The variables d_{42}, d_{31} and d_{53} are distances between vertices of the unit cell. In terms of the unit cell parameters the density ρ_{2-2} is determined from geometry of the unit cell (Figure 2), as for the buckling transition discussed above.

Evolution of the first two layers and formation of a third layer. *Buckling transition* (*2*Δ → *3*□). Figure 3 demonstrates the buckling transition occurring with increase in pore width when the number of adsorbed layers increases from two layers to three layers. This transition can be modeled in stages. In the early stage of the transition at the smaller pore size shown in the Figure 3a, adsorbates belonging to the third layer do not lie on the same plane since there is a stronger attraction between the nearest pore wall and the adsorbate and between adsorbates within each layer, than between the more distant pore wall and the adsorbates and between adsorbates in different layers. In this stage, second nearest neighbors or higher order rather than only nearest neighbors should be taken into account for an accurate solution as the molecules are relatively close to each other. However, this complexity may be avoided if the unit cell parameter d is assigned to be $2^{1/6}\sigma_{ii}$ at this stage. With this simplification it was found that the predicted results matched reasonably well the simulated ones, as will be discussed subsequently.

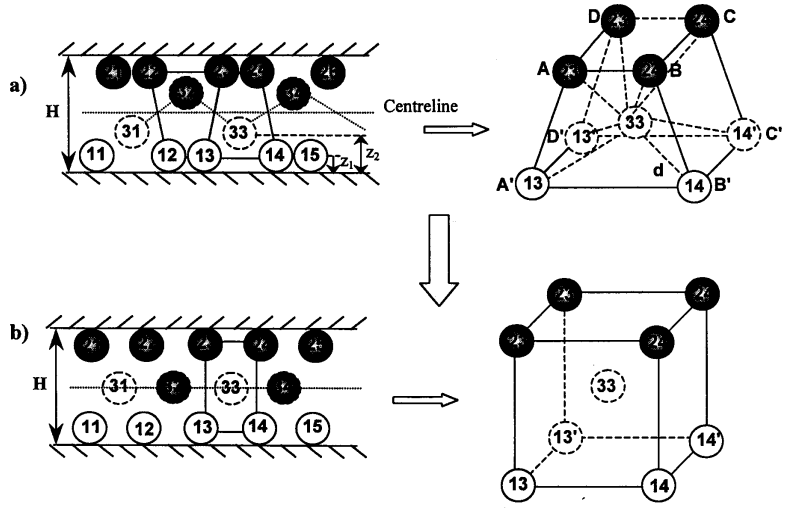

Fig. 3. (a) Adsorbed molecules from the first two layers contribute to the formation of a third layer. At the pore width where the third layer starts to form, these adsorbed molecules do not lie on the same plane. For sufficiently large pore widths, the adsorbed molecules lie on the same plane. The selected unit is body-centered cube (bcc) instead of face-centered cube (fcc).

In the final stage of the transition at larger pore width shown in the Figure 3b, adsorbates belonging to the third layer locate at the pore center. Furthermore, the adsorbates, in this stage, are relatively far apart. Consequently, only consideration of nearest neighbors is necessary to obtain reasonable match to GCMC simulation.

From Figure 3, the total interaction energy is given by

$$E = 8\Phi_{ii}(d) + 2\Phi_{ii}(d_1) + 2\Phi_{ii}(d_2) + 2\Phi_{ii}(d_1\sqrt{2}) + 2\Phi_{ii}(d_2\sqrt{2}), \tag{19}$$

where d, d_1 and d_2 as described in the Figure 3

The density is derived from geometry of the unit cell (Figure 3), similar to that discussed above

Rhombic transition (*3□→ 3*Δ)**.** In this transition, depicted in Figure 3b, the first and second layers are relatively far apart and the third layer is assumed to be located at the pore center. Thus, if only nearest neighbors have been taken into account, the body centered cube can be split into two identical cubes, which are described in the Figure 2. These cubes are symmetrical through the centerline of the pore.

The total interaction energy E of the unit cell is given

$$E = N\left[2\Phi_{ii}(d_1) + \Phi_{ii}(d_{42}) + \Phi_{ii}(d_{31}) + 1.5\Phi_{ii}(d) + 0.5\Phi_{ii}(d_{53})\right], \tag{20}$$

Free energy minimization. Equations (3), (4) and (6) provide the grand potential of the unit cell

$$\Omega = E + Nv_{ex} - NkT\left[\ln\left(\frac{1}{\lambda}\frac{N^*}{a}\right) - 1\right], \tag{21}$$

where the external potential v_{ex} follows eq. (12). The unit cell potential energy E corresponding to any structure is obtained as discussed in next sections. Through these, the grand potential can be expressed in terms of the parameters z, d_1, d_2.

The equilibrium structures will corresponding to a minimum in free energy with respect to the characteristic parameters of the unit cell, which are, for instance, z, d, α in the case of buckling transition from monolayer to second layer. Thus, d, z, α are the roots of

$$\left(\frac{\partial\Omega}{\partial z}\right)_{d,\alpha} = \left(\frac{\partial\Omega}{\partial d}\right)_{z,\alpha} = \left(\frac{\partial\Omega}{\partial \alpha}\right)_{z,d} = 0 \tag{22}$$

The set of nonlinear equations resulting from the above minimization is solved by using the Newton Raphson technique.

3. GRAND CANONICAL MONTE CARLO SIMULATION TECHNIQUE

Grand canonical Monte Carlo simulation (GCMC) is widely used to determine amount adsorbed in the confined space. In GCMC simulation temperature, chemical potential and volume μ, V, T are kept constant while number of particles and associated configurational energy are allowed to fluctuate. In this study, GCMC simulation was used to generate values for the capacity of methane in slit-pores. In the simulation, the adsorbate-adsorbate interaction potential was modeled using a Lennard-Jones potential truncated at 1.5 nm. The parameters of CH_4 and CF_4 were the same as those used in the DFT calculations.

The adsorbent-adsorbate interaction potential of each wall in the graphitic slit-pore was represented by Steele's 10-4-3 potential. The size of the simulation box was set to $20\sigma_{ff}$ and the number of configurations varied from $1x10^7$ to $2x10^7$. To ensure high filling densities, a pressure of (50-55) bars at (180^oK-200^oK) was chosen for pore widths up to 2 layers and (252-276) bars for pores that can accommodate 3 layers. The high densities obtained under these pressures can be reasonably taken to be the maximum capacity, since the density increases insignificantly (<5%) when much higher pressures are used. This issue will be discussed further later. GCMC simulation were also run at 150^oK, 250^oK and 308^oK to investigate the temperature effect on density at the high pressure limit.

4. RESULTS AND DISCUSSION

Simulation results. Figures 4(a-d) and 5(a-b) depict the GCMC simulation results for capacity methane and carbon tetraflouride in slit-shaped pores as a function of pore width. In the Figures the symbols represent the GCMC results and lines the model prediction to be discussed subsequently. From these Figures, it is observed that the capacity fluctuates with pore width in region (I) corresponding to pores whose size accommodates three layers at maximum. From this region onwards, density fluctuations gradually die out. This shows that the dependence of capacity on pore width is not trivial in activated carbon. The dependence of capacity on pore size is due to the fact that the packing configuration of the adsorbed phase changes continuously as pore size is enlarged. From Figures 4 and 5 it is also evident that the assumption of $d = 2^{1/6}\sigma_{ii}$, for the buckling transition $2\Delta \rightarrow 3\square$, is satisfactory and provides good agreement with simulation. Figures 6 and 7 show that the packing configuration of the adsorbed phase passes continuously through a sequence of crystalline structures during a buckling transition (hexagonal monolayer to two square-packed layers to two hexagonal-packed layers). The pair distribution function obtained by GCMC simulation also facilitates identification of the

packing configuration of an adsorbed phase, since the position of the peaks in the pair distribution profile corresponds to the location of neighbors around a central molecule. For example, peaks representing increasingly distant neighbors around a central molecule in a hexagonal configuration are located at, $r_o, \sqrt{3}\, r_o, 2r_o, \sqrt{7}\, r_o$ and in a square configuration, at $r_o, \sqrt{2}\, r_o$, $2r_o$, $\sqrt{5}\, r_o$, $2\sqrt{2}\, r_o$ where r_o is the nearest neighbor separation. Figures 7 and 8 show pair distribution function profiles characteristic of hexagonal and square configurations respectively.

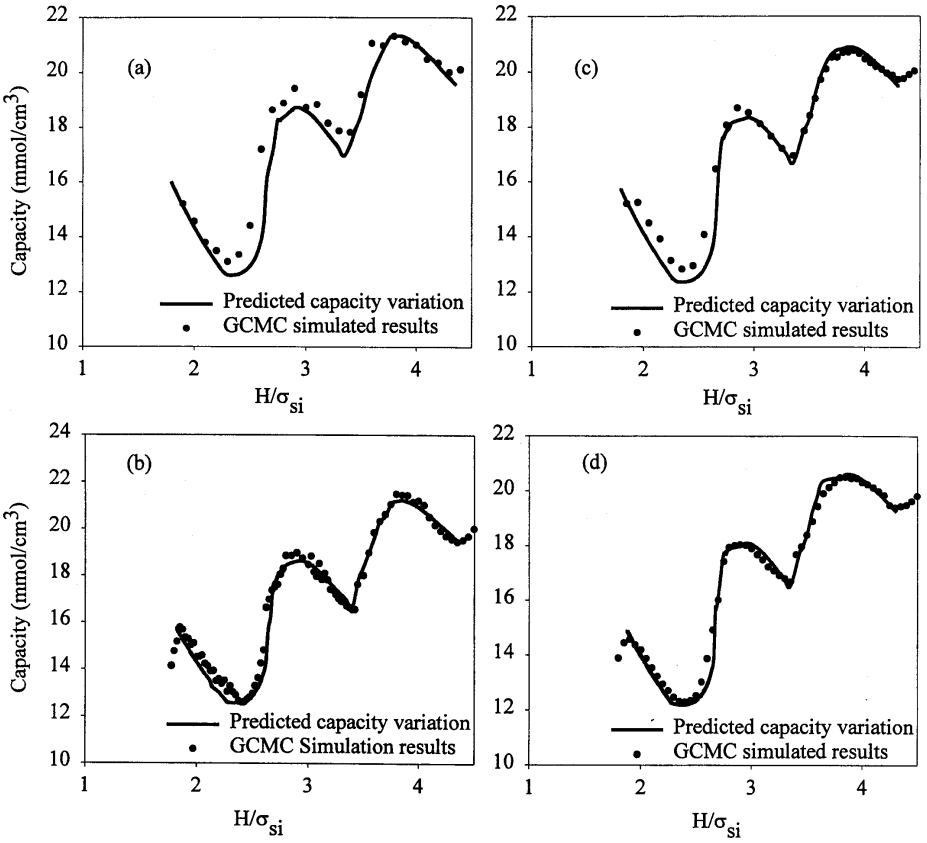

Fig. 4. Comparison of predicted capacity profiles of methane with GCMC simulated ones at four different temperatures corresponding to sub-critical and supercritical conditions: (a) 150°K; (b) 180°K; (c) 250°K and (d) 308°K.

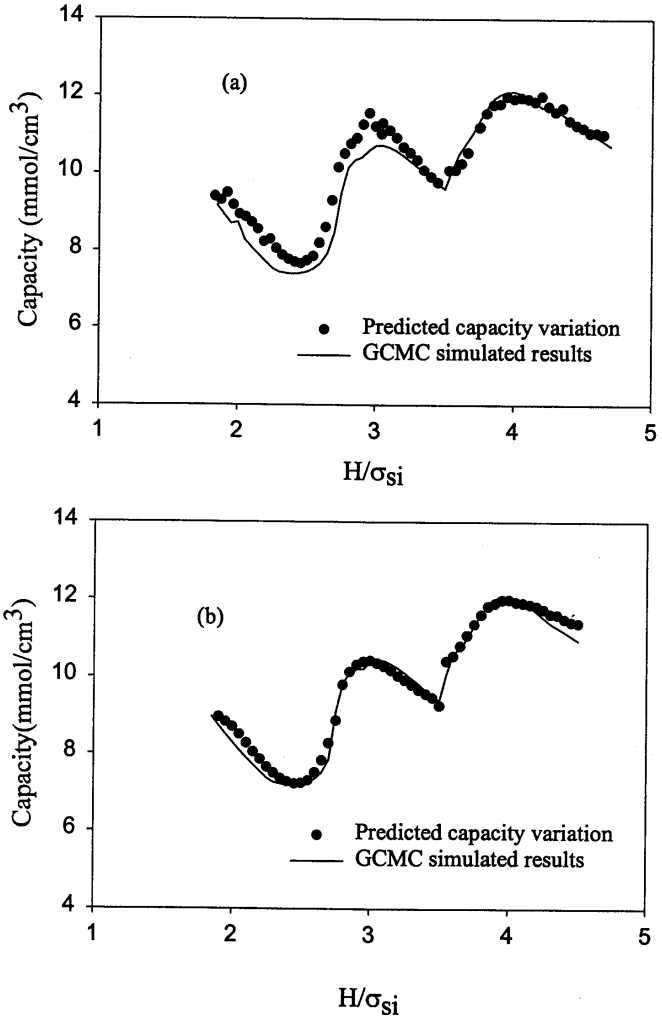

Fig. 5. Comparison of predicted capacity profiles of carbon tetraflouride with GCMC simulated ones at four different temperatures corresponding to sub-critical and supercritical conditions: (a) 200 ^{o}K and (b) 308 ^{o}K.

Transitions and microstructure of adsorbed phase. The results extracted from the model proposed in Section 2 explain the microstructure of an adsorbed phase. Before a detailed interpretation of microstructure of adsorbed phase is given, the capacity profile obtained by GCMC simulation is compared with those predicted by the proposed model up to three layers. For higher layers, the transitions of the adsorbed phase between square and hexagonal configurations become increasingly complex due to an increase in the number of possible packing configurations.

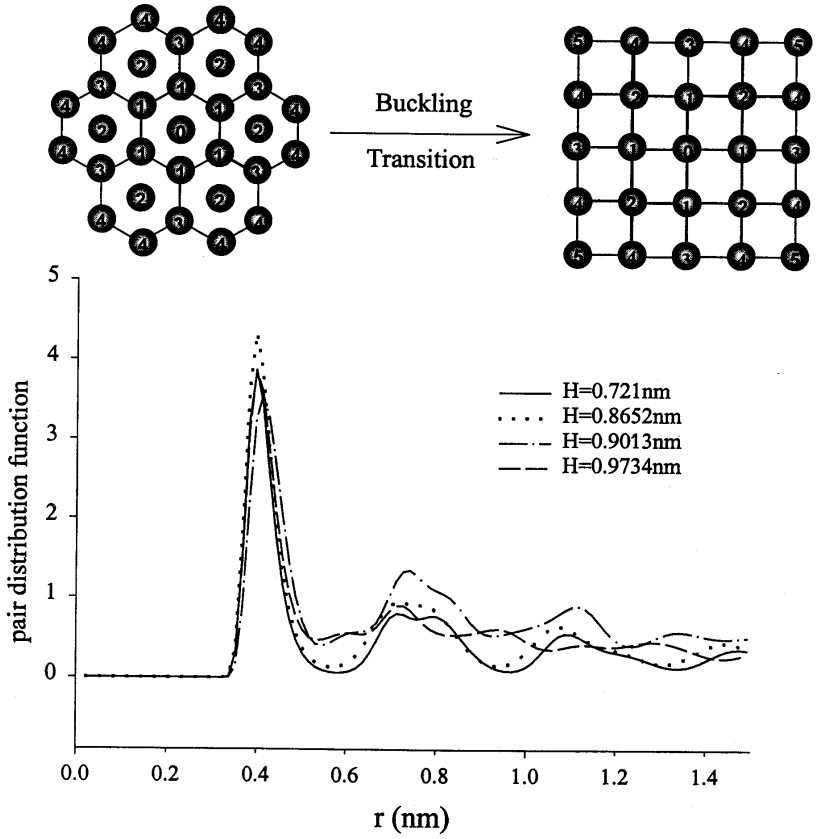

Fig. 6. Pair distribution function obtained by GCMC simulation, depicting the structural variation during buckling transition.

However, the capacity fluctuation of methane and larger molecules become less significant as pore size is enlarged beyond three layers. Moreover, a predominant proportion of pore sizes less than three layers is normally observed in microporous carbons. From Figures 4 and 5, it is seen that the predicted capacity profiles match the simulated ones very well. However, a small deviation between predicted capacity profiles and the simulated ones at 200^{o}K but not 308^{o}K was observed for carbon tetraflouride (Figure 5a). This may arise from large molecules that may give rise to the stronger fluid-fluid interaction between the central molecule and its neighbors, particularly for small pore size at low temperature.

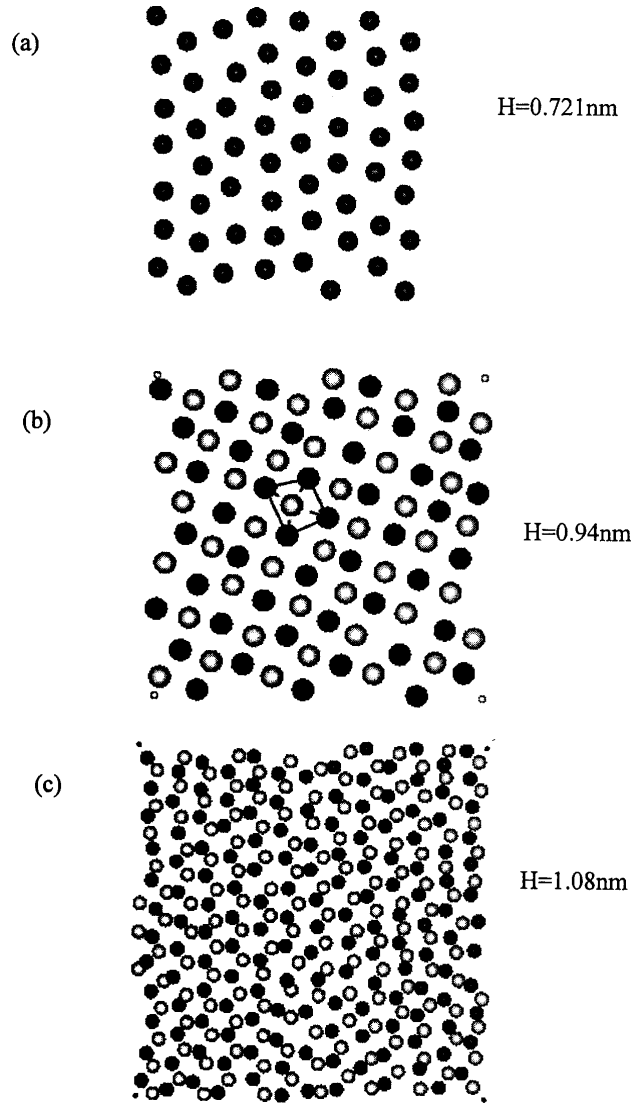

Fig. 7. Snaphshots of structural variation of the adsorbed phase of methane during the buckling transition. (a) Monolayer in hexagonal configuration; (b) two layers in square configuration; (c) two layers in hexagonal configuration. Filled and empty circles represent adsorbed molecules in each layer.

However, the fluid-fluid interaction between a central molecule and it's higher neighbors becomes weaker at high temperature at which adsorbed molecules are relatively far apart. Consequently, the predicted density profile matches the simulated results very well (Figure 5b).

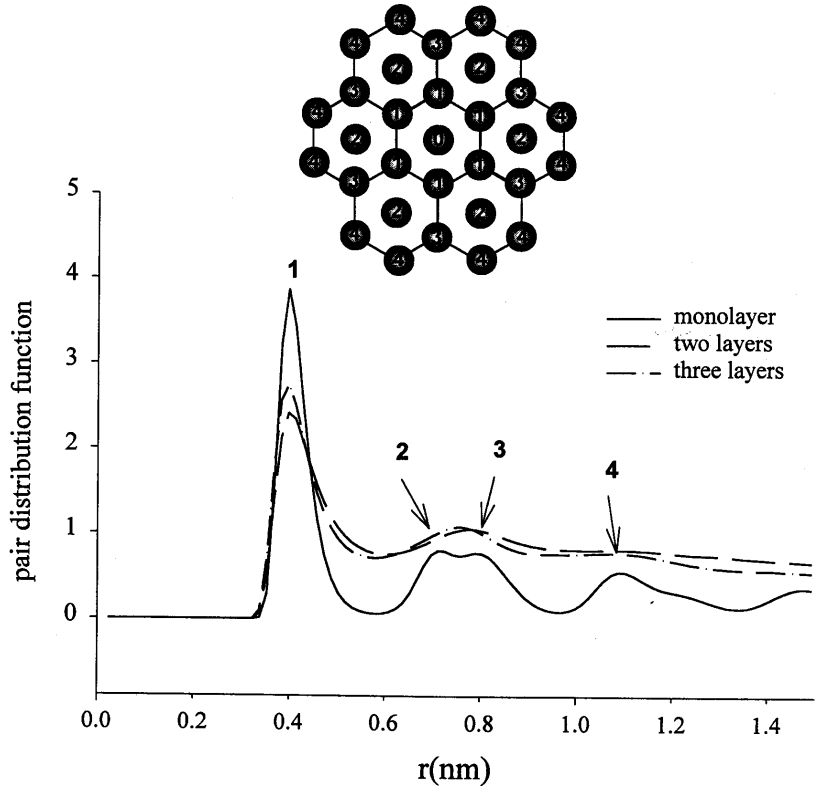

Fig. 8. Pair distribution functions of methane obtained by GCMC simulation corresponding to hexagonal packing configuration of the adsorbed phase, in pores that accommodate exactly one layer, two layers and three layers respectively. (1) nearest neighbors, (2) second nearest neighbors, (3) third nearest neighbors, (4) fourth nearest neighbors.

Owing to similar transitions observed for methane and carbon tetraflouride, the interpretation of the closed packed transitions and microstructure of adsorbed phase are conducted for methane and then compared with carbon tetraflouride in appropriate sections. For convenient reference, the interpretation is divided into sections corresponding to specific configurations and transitions as follows:

Monolayer. *Region I,* (*H <0.818nm*). In this region, the characteristic parameters of the unit cell, *z*, *d*, and α are independent of pore size. *z* is found to be half pore size. This results from the coalescence of the two minima of the grand potential into one minimum located in the center of the pore.

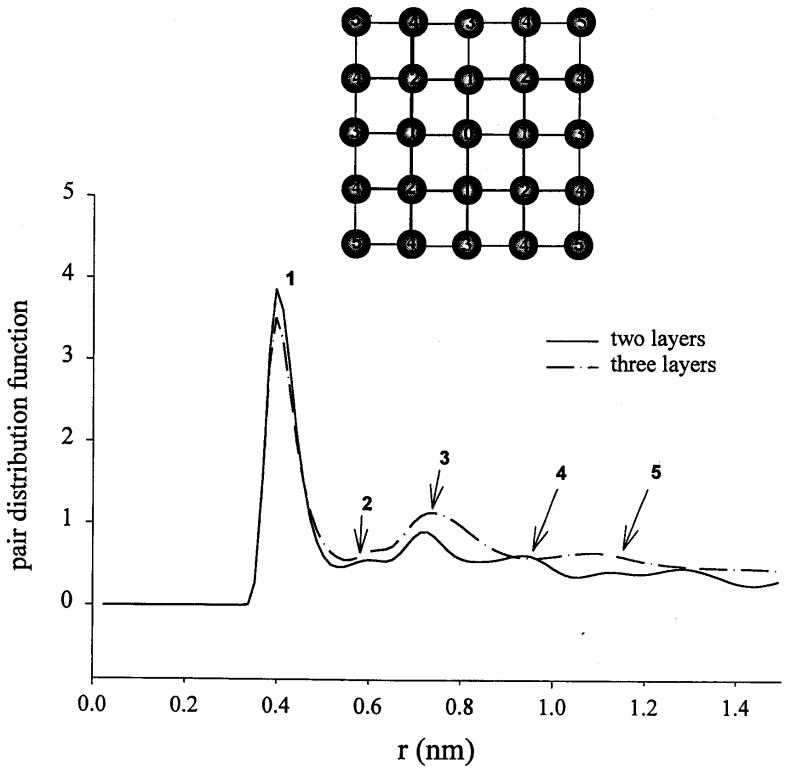

Fig. 9. Pair distribution functions of methane obtained by GCMC simulation corresponding to square packing configuration of the adsorbed phase, in pores that accommodate two layers and three layers respectively.

For methane, the predicted value d=1.1977 σ_{si} is found to be close to the simulation value 1.1692 σ_{si}, which is the location of the first peak of the pair distribution profile obtained by GCMC simulation for nearest neighbors (Figure 8). The similar result were found in the case of carbon tetraflouride.

It is interesting that the values d of methane and carbon tetraflouride being 1.1977σ_{si} and 1.3173σ_{si} respectively approximate to $2^{1/6}\sigma_{ii}$ where minimum L-J pair potential is present. This indicates that fluid-fluid interaction plays key role in determining density in the monolayer region. Consequently, it is very difficult to push adsorbed molecules closer together than this distance because of repulsive forces. This is in contradiction to the surface compression mechanism proposed by Aranovich and Donohue [21]. In addition, the parameters α of methane and carbon tetrafloride being α=0.5747 and 0.5709 are close to the value 0.5774 obtained by GCMC, which corresponds to a hexagonal configuration of the dense monolayer. Thus, a hexagonal packing configuration is energetically favored in this region. In Figure 7a, the snapshot

of the monolayer of methane in a pore of 0.721nm obtained by GCMC confirms that the monolayer is packed in a hexagonal configuration.

Second layer. *Region II* (*0.82 nm<H<1.00 nm*). In this region, the parameter α, which is the ratio d_2 to d_1 (Figure 2) , is found to increase gradually from 0.5747 to 0.7952 while the parameter d decreases steadily from $1.1977\sigma_{si}$ to $1.1636\sigma_{si}$ with increasing pore width. There exist two roots for the parameter z that represent the locations of the first and second layers. This shows that the formation of the second layer is associated with the evolution of a hexagonal configuration to a square one. The parameter d decreases to less than $2^{1/6}\sigma_{ii}$ during second layer formation due to the contribution of solid-fluid interaction of two opposite pore walls, indicating that the adsorbed molecules pack more efficiently in the intermediate configurations between perfect hexagonal and square configurations. This is one important feature of fluids in confined geometry, which is not observed in bulk fluids. It is interesting that the parameter α jumps from 0.7952 to 1 corresponding to a perfect square configuration instead of increasing steadily to 1. Figure 7b shows the snapshot of a square configuration obtained from a GCMC simulation at the pore width of 0.94 nm in agreement with the square configuration (α =1) predicted from the model. Moreover, variation in pair distribution functions (Figure 6) obtained by GCMC simulation confirms that there is a continuous passage from the hexagonal configuration to the square one through intermediate configurations during the buckling transition. Thus, in this region the buckling transition from hexagonal to square configurations is the energetically favored path, similar to that in a hard sphere systems [9]. The similar results were found for carbon tetraflouride.

Region III (*1.00 nm<H<1.23 nm*). In this region, it is expected that there will be rhombic transition of the adsorbed layers, from a square configuration to a hexagonal one, without the formation of a new layer. To demonstrate the transition, we investigated the evolution of the ratio α of d_{13} to d_{42}, which are two diagonal lines of cross-section in each layer. By solving the model in this region it is found that α equals unity when H=1.0094 nm, indicating a perfect square configuration of the adsorbed layers. As the pore width is slightly enlarged to 1.0274 nm, α jumps from 1 to 1.79 and then approaches 1.73, corresponding to a perfect hexagonal configuration. Thus the square configuration is less energetically favored than the hexagonal one when the pore width exceeds 1.0094 nm. Beyond a pore width of 1.0274 nm, α decreases gradually to 1.73 corresponding to a perfect hexagonal configuration, indicating that the adsorbed layers pass continuously through the intermediate structures before reaching the perfect hexagonal configuration. The characteristic para-

meter for a hexagonal configuration d_1 equals $1.2022\sigma_{si}$, which is slightly higher than that obtained in region I ($1.1977\sigma_{si}$). This may be due to a weaker grand potential resulting from separation of its minima.

Third layer. *Region IV* (*1.23 nm<H<1.442 nm*). In this region, the third layer is formed in association with variation in structure of each adsorbed layer, i.e. a buckling transition. Modeling of this transition is more complex. To describe this transition, we model the unit cell as a body-centered cube (bcc) (Figure 3) instead of the face-centered cube (fcc), which has been observed in bulk solid xenon and solid xenon confined in large slit-pore by Donnelly [22]. It is found that coordinates of adsorbed molecules within the third layer z_2 (H<1.33 nm) do not lie on the pore center. This shows that adsorbed molecules in the third layer do not lie in the same plane until the pore width is sufficient large (~1.298 nm) corresponding to a perfect body-centered cube. In Figure 4 it is observed that the model matches the simulated data reasonably well for methane and carbon tetraflouride, indicating the suitability of the model of body-centered cube to describe the transition.

Region V (*1.34 nm <H<1.60 nm*). In this region, there is a rhombic transition in which the square configuration of each layer is continuously deformed into a hexagonal configuration. Again the transition also evolves as described for region III. Each adsorbed layer begins with a square configuration at pore width 1.34 nm and deforms continuously into the hexagonal configuration. At the end of the transition, a nearly perfect hexagonal configuration in each layer is obtained at a pore width 1.6 nm. The characteristic parameter for the hexagonal configuration is found to be $1.2038\sigma_{si}$, which is slightly higher than the values obtained for the first and second layers, indicating weaker solid-fluid interaction with increasing distance between two walls of the pore.

5. CONCLUSIONS

In this paper we conducted an application of the model [10] to methane and carbon tetraflouride in graphitic slit-pores. The model is based on a density functional theory approach applied at the close packed limit. The grand potential of the unit cell of the adsorbed phase is optimized in terms of its characteristic dimensions rather than that of the whole adsorbed phase. The model does not require any fitting parameters to obtain the capacity.

The model was compared with results from GCMC simulation and excellent agreement was found up to three layers. From the characteristic dimensions extracted from the model, the microstructures of the adsorbed phase associated with the structural transitions occurring in the pore as the pore width is enlarged

can be elucidated. The model shows that adsorbed molecules in a confined space can pack closer than $2^{1/6}\sigma_{ii}$ in the intermediate configurations. Furthermore, the hexagonal configuration seems to be energetically favored and thermodynamically stable and is always the final configuration of the newly-formed layer.

Although the model provides a successful prediction of the capacity profile, it is more difficult to extend the model beyond 3 layers, since geometrical transitions in the adsorbed phase at higher layers are not unique. However, the variation in density with pore width, although very significant up to three layers, attenuates quickly at higher layers.

Acknowledgement. This research has been supported by a grant from the Australian Research Council, under the discovery scheme. D.N. would like to thank the University of Queensland for a Travel Support Grant.

REFERENCES

[1] Pieranski, P. and L. Strzelecki (1983), "Observation of Quantum Diffractive Velocity-Changing Collisions by Use of Two-Level Heavy Optical Radiators," *Physical Review Letters*, 50, 331.
[2] Murray, C.A. (1990), "Comparison of melting in three and two dimensions: Microscopy of colloidal spheres," *physical Review B*, 42, 688.
[3] Murray, C.A. (1992), in *Bond-Orientational Order in Condensed Matter Systems*, K.J. Strandburg, *ed*. New York: Springer.
[4] Weis, J., et al. (1995), *Chemical Physics*, 103, 1180.
[5] Schmidth, M. and H. Lowen (1997), "Phase diagram of hard spheres confined between two parallel plates," *Physical review E*, 55, 7228.
[6] Davies, G.M. and N.A. Seaton (1998), "The effect of the choice of pore model on the characterization of the internal structure of microporous carbons using pore size distributions," *Carbon*, 36, 1473-1490.
[7] Nicholson, D. and T. Stubos (2000), "Simulation of adsorption in micropores, "*Recent Advances in Gas Separation by Microporous Ceramic Membranes*,, 231-256.
[8] Cracknell, R.F., et al. (1996), "Adsorption and selectivity of carbon dioxide with methane and nitrogen in slit-shaped carbonaceous micropores: Simulation and experiment," *Adsorpt.-J. Int. Adsorpt. Soc.*, 2, 193-203.
[9] Pansu, B., P. Pieranski, and P. Pieranski (1984), "Structures of thin layers of hard spheres : high pressure limit," *Journal of Physique (Paris)*, 45, 331.
[10] Nguyen, T.X., S.K. Bhatia, and D. Nicholson (2002), "Close packed transitions in slit-shaped pores: density functional theory study of methane adsorption capacity in carbon," *Journal of Chemical Physics (submitted)*,,
[11] Tan, Z. and K.E. Gubbins (1992), *Physical Chemistry*, 96, 845.
[12] Sokolowski, S. and J. Fischer (1990), "The role of attractive intermolecular forces in the density functional theory of inhomogeneous fluids.," *Mol. Phys.*, 70, 1097.
[13] Tarazona, P. (1985), "Free-energy density functional for hard spheres," *Physical review*, 31, 2672.
[14] Kierlik, E. and M.L. Rosingberg (1991), "Density functional theory for inhomogeneous fluids : Adsorption of binary mixtures," *Physical Review A*, 44, 5025.

[15] Patra, C.N. and S.K. Gosh (1997), *Chemical Physics*, 106, 2752.
[16] Sowers, S.L. and K.E. Gubbins (1995), *Langmuir*, 11, 4758.
[17] Maddox, M.W., S.L. Sowers, and K.E. Gubbins (1996), *Adsorpt.-J. Int. Adsorpt. Soc.*, 2, 23.
[18] Evans, R. (1979), "The nature of the liquid-vapour interface and other topics in the statistical mechanics of non-uniform, classical fluids," *Advances in Physics*, 28, 143.
[19] Steele, W.A. (1973), *Surf. Sci.*, 36, 317.
[20] Johnson, E. (2002), "The elusive liquid-solid interface," *Science*, 296, 477-478.
[21] Aranovich, G.L. and M.D. Donohue (2001), "Surface compression in adsorption systems," *Colloids and surfaces A: Physicochemical and engineering aspects*, 187-188, 95-108.
[22] Donnelly, S.E., et al. (2002), "Ordering in a fluid inert gas confined by flat surfaces," *Science*, 296, 507-510.

CURRICULUM VITAE

Prof. Bhatia obtained his B.Tech. from the Indian Institute of Technology, Kanpur, and his M.S.E. and Ph.D. degrees from the University of Pennsylvania, in-between serving in industry for two years. After another stint in industry he returned to academia. Between 1984 and 1996 he was at the Indian Institute of Technology, Bombay, before joining the University of Queensland where he is Professor in Chemical Engineering. His main research interests are in adsorption and transport in nanoporous materials and in heterogeneous reaction engineering, where he has authored over one hundred scientific papers in leading international journals. He is a Fellow of the Indian Academy of Sciences and recipient of the Herdillia Award for Excellence in Basic Research in Chemical Engineering from the Indian Institute of Chemical Engineers, in 1992. In 1993 he was awarded the Shanti Swarup Bhatnagar Prize for Engineering Sciences by the Government of India.